NJC

Accepted Manuscript

This is an *Accepted Manuscript*, which has been through the Royal Society of Chemistry peer review process and has been accepted for publication.

Accepted Manuscripts are published online shortly after acceptance, before technical editing, formatting and proof reading. Using this free service, authors can make their results available to the community, in citable form, before we publish the edited article. We will replace this *Accepted Manuscript* with the edited and formatted *Advance Article* as soon as it is available.

You can find more information about *Accepted Manuscripts* in the Information for Authors.

Please note that technical editing may introduce minor changes to the text and/or graphics, which may alter content. The journal's standard Terms & Conditions and the Ethical guidelines still apply. In no event shall the Royal Society of Chemistry be held responsible for any errors or omissions in this *Accepted Manuscript* or any consequences arising from the use of any information it contains.

ROYAL SOCIETY OF CHEMISTRY

www.rsc.org/njc

New Journal of Chemistry RSCPublishing

ARTICLE

THICKNESS CONTROL OF GRAPHENE DEPOSITED OVER POLYCRYSTALLINE NICKEL

Cite this: DOI: 10.1039/x0xx00000x

Received ooth January 2012,
Accepted ooth January 2012

DOI: 10.1039/x0xx00000x

www.rsc.org/

Mª del Prado Lavin-Lopez,[a] Jose Luis Valverde,[b] Mª Inmaculada Ruiz-Enrique, [b] Luz Sanchez-Silva[b] and Amaya Romero[b]

The optimization of the graphene growth over polycrystalline nickel foils using an atmospheric pressure Chemical Vapor Deposition set up is reported. CH_4 and H_2 were used as precursor gases. Optical Microscopy and Raman spectroscopy were used for graphene characterization. A *thickness value* related to number of graphene layers in the synthesized samples was quantified using an Excel-VBA application, which assigned a *thickness value* between 0 and 1000 and allowed to know the percentage of each type of graphene (monolayer, bilayer, multilayer) deposited over the Ni foil. The influence of reaction temperature, CH_4/H_2 flow rate ratio and reaction time was studied in detail. Optical Microscopy showed that samples were not homogeneous, being covered with multilayer, few-layer, bilayer and monolayer graphene. Synthesis variables were optimized according to the *thickness value*. It was observed a maximum *thickness value* (781) for a temperature, a CH_4/H_2 flow rate ratio and a reaction time of 980 ºC, 0.07 v/v and 60 seconds, respectively. At these conditions, about 77% of the Ni foil was covered with monolayer graphene.

Introduction:

Graphene, a two dimensional carbon network with a hexagonal crystal structure of sp^2-bonded carbon atoms, has been gained attention for its unique structure. Its exceptional properties [1-5] such as its theoretical specific surface area that is up to 2600 m^2/g [6], the value of its thermal conductivity, around 3000 W/m K, its speed electron mobility at room temperature around 15000 $cm^2/V\ s$ [7], its mechanical stress, around 1060 GPa [8], and its density, which is 2.2 g/cm^3 [(7)]. In addition, graphene is reported to own other extraordinary characteristics such as anomalous quantum Hall effect, bipolar supercurrent chiral tunnelling of relativistic particles and absence of Anderson location [7].

Due to these characteristics and properties, graphene could have application in a variety of fields such as field effect transistors manufacture, transparent conductive films, clean energy devices, graphene-polymer nanocomposites, biotechnology, composites, batteries, electronic, solar cells and sensors[9].

There are several methods to synthesize graphene such as *arc discharge* [10, 11], *epitaxial growth on SiC* [12-17], *unzipping carbon nanotubes* [18-20], *CO reduction* [21], *chemical conversion* [22], *self-assembly of surfactants* [23] and *Chemical Vapor Deposition (CVD)* [24-28]. Graphene or modified graphene sheets can be also produced by *separation/exfoliation of graphite or graphite derivate* like graphite oxide (GO) and graphite fluoride [29].

Recently, Chemical Vapour Deposition (CVD) technique, using copper or nickel as catalyst, has displayed great advantages since it leads to the manufacture of wafer scale of near-perfect quality graphene[30, 31].

The layer-controlled surface growth of large-area graphene films have been actively pursued due to their variety of properties and applications in different fields and its compatibility with manufacture technologies.

In CVD, a metal substrate is put into a furnace and heated to high temperatures. The heat anneals the metal, increasing its domain size[32]. Methane and hydrogen gases are flowed through the furnace. Hydrogen catalyses the reaction between methane and the metal substrate, resulting carbon atoms, which are deposited onto the metal surface. After the reaction, the furnace is cooled to avoid the aggregation of the deposited carbon atoms, which crystallizes into a continuous graphene layer on the metal surface [33].

Using the *CVD method,* few layers of graphene can be obtained with a lateral of graphene sheets very large (cm in size). Thus CVD method allows to produce high quality and large size graphene at wafer scale [30] being considered a low cost and a high yield method if compared to other growth methods. However, the graphene growth from CVD tends to wrinkle due to the difference in thermal expansion between graphene and metal layer. This could be decreased via proper annealing, but it is still an ongoing research challenge[32].

Nickel and copper are commonly used in the CVD method as the metal substrate material for graphene synthesis[34]. Due to the high solubility of carbon in nickel, the precipitation of extra-carbon occurs at the metal surfaces during cooling [35]. Since the segregation is a non-equilibrium process, this makes thickness control of graphene a challenge [35]. Other transition metals such as Ru, Co and Pt are alternative transition metals although they are used less frequently[36, 37].

In the case of Ni, graphene growth occurs after methane gas decomposition, causing the diffusion of carbon atoms through the metal surface forming a solid solution. After that, carbon atoms segregate from inside of the metal to the metal surface and then precipitate, forming graphene layers. It has been reported that carbon segregation on nickel is non-uniform at low-temperature[35]. However, the high decomposition temperature of methane, favoured a constant carbon coverage over the nickel surface[35]. Furthermore, high melting point of nickel enables high-temperature annealing, which results in larger domains, thus making it favourable for large-area low-defects growth[38]. Mono-crystalline nickel favours crystal formation on its surface obtaining more uniform monolayer and bilayer graphene with smooth surface and with practically no defects. Simultaneously, it prevents the formation of multiple layers on the grain boundaries. Conversely, poly-crystalline Ni has a rougher surface, where the presence of grain boundaries facilitates the formation of multilayer graphene. However, mono-crystalline metals are more expensive than poly-crystalline ones. From a large-scale production point of view, the use of poly-crystalline Ni is more profitable, being the researches focused on improving the conditions of the main variables that influence over the reproducible synthesis of high quality graphene at large scale[39]. Several studies have demonstrated a close correlation between the CVD growth parameters, the number of graphene layers and the quality of the synthesized graphene, which enables the formation of monolayer, bilayer, few-layers and multilayer graphene on Ni substrates. Lavin-Lopez *et al. (2014)* found that the growth temperature significantly influenced over the graphene quality [40]. The thermodynamically driven precipitation can be kinetically controlled to some extent. For example, low temperature and low hydrocarbon exposures have been employed successfully to control carbon diffusion to the surface and thus, leading to the monolayer, bilayer, few-layer or multilayer graphene formation [41]. The high carbon solubility in nickel implies that the conditions for monolayer growth require low precursor pressures and temperatures [41].

The aim of this work was to optimize the graphene growth over polycrystalline nickel foils using a homemade atmospheric pressure Chemical Vapor Deposition setup. CH_4 was used as the precursor gas whereas H_2 and N_2 were used as carrier gases. Thus, different growth operation conditions, presumably affecting the CVD-grown graphene characteristics, e.g. reaction temperature, CH_4/H_2 flow rate ratio in the feed and reaction time, were studied in detail.

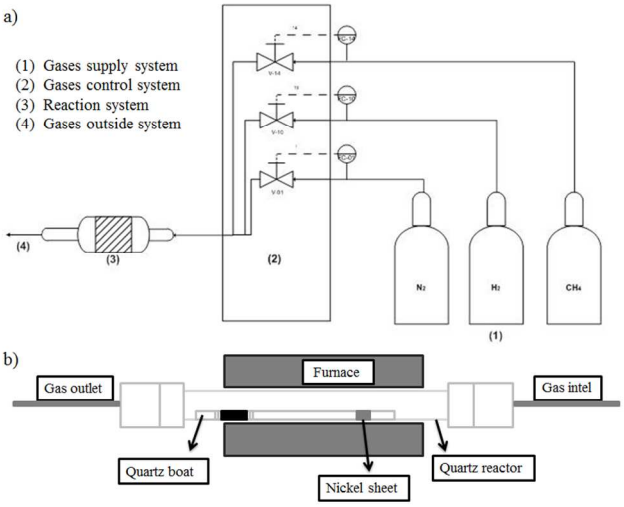

Fig 1. Set-up used for the CVD synthesis of graphene on polycrystalline nickel

The resulting materials were characterized by Raman spectroscopy in order to evaluate both the number of graphene layers and the defects present in them[42]. Furthermore, a homemade Excel-VBA application allowed to analyse the thickness of the graphene samples and thus, evaluate the percentage of each type of graphene covering the polycrystalline nickel sheet [40].

Experimental:

Materials:

25 µm thick polycrystalline nickel sheets with a high purity grade (99.99%) were purchased from GOODFELLOW. Hydrogen and nitrogen with high purity grade (99.999%) and methane (99.5 %,) were supplied by Praxair.

Method:

Graphene samples were grown at atmospheric pressure on 25 µm thick polycrystalline nickel foils in a 40-inch quartz tube heated by a furnace (Figure 1) using the CVD method[27]. The furnace was heated to 900 ˚C by passing through it a flow of N_2 (400 sccm) and H_2 (100 sccm) to prevent nickel oxidation. The furnace was maintained at 900 ˚C for 45 minutes to allow the annealing of the polycrystalline nickel foil. Then, its temperature set point was set at a value ranging from 900 and 1050 ºC, depending on the selected reaction temperature. Next, 30 sccm of a mixture of methane and hydrogen (CH_4/H_2 flow rate ratio in the range 0.4-0.07 v/v) was introduced during a time ranging from 30 second to 900 seconds. Finally, the system was cooled (10˚C min^{-1}) by flowing 400 sccm of nitrogen. The synthesis process is summarized in Figure 2. Repetitiveness studies were performed demonstrating that as-synthesized samples characteristics were reproducible.

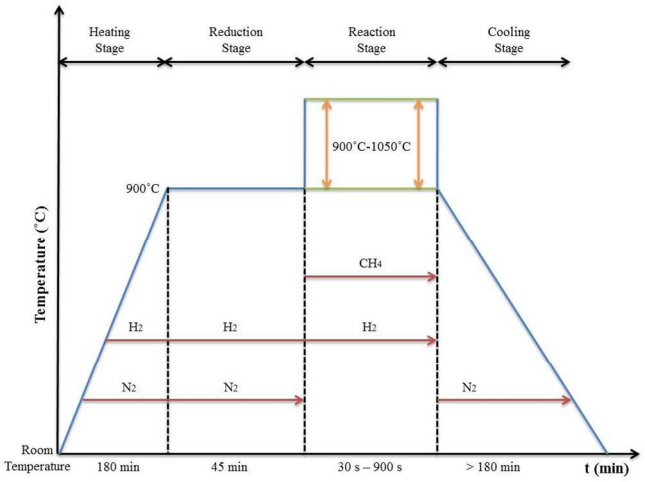

Fig 2. Summary of the stages times, temperatures and gases used during graphene synthesis.

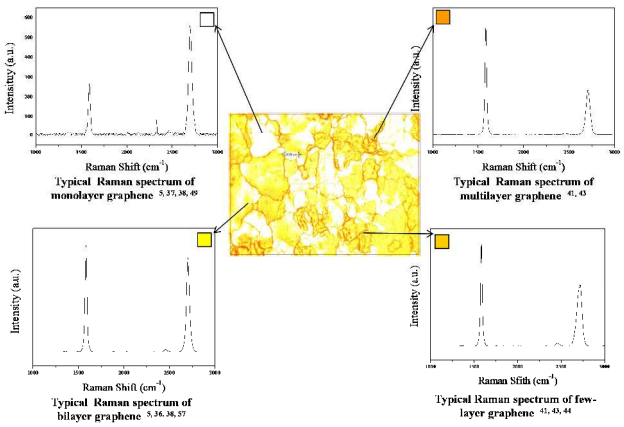

Fig 3: Relation between the different colours present in an Optical Microscopy image and the type of graphene present in the sample by Raman spectroscopy.

Characterization:

Raman spectroscopy:

A SENTERRA Raman spectrometer with 600 lines per mm grating and 532 nm laser wavelength at a very low laser power level (<1mW) to avoid any heating effect was used to characterize the different graphene samples. Raman spectroscopy is considered as a reliable and quick method to characterize graphene[43-46]. D peak, visible at ~ 1350 cm^{-1}, is related to the presence of defects (edges, dislocations, cracks or vacancies) in graphitic materials [46]. Two more peaks named G and 2D bands are visible at around 1580-1620 cm^{-1} and ~ 2700 cm^{-1}, respectively. G peak denotes the symmetry-allowed graphite band and, is a way of checking the vibration on the same plane of sp^2 hybridized carbon atoms, which compose graphene sheets [46]. 2D peak, originated from second order double resonant Raman scattering from zone boundary, is the hallmarks of different numbers of graphene layers[47, 48].
The amount of defects present in graphene samples can be quantified by measuring the intensity ratio of D and G bands (I_D/I_G). On the other hand, the number of graphene layers is directly related to the ratio of G and 2D bands (I_{2D}/I_G). These parameters are characteristics of CVD-grown of graphene[49]. Other remarkable parameters in the characterization of graphene are the following ones: ***FWHM*** (Full Width at Half Maximum) and ***2D and G peak position*** (Raman Shift, cm^{-1}). FWHM is related to the life-time of the excited states (life-time for the Raman scattering process), which is the time delay between the absorption of the incident photon and the emission of the outgoing one [5], which is calculated as the Raman Shift difference to the half average height of 2D band. On the other hand, *G peak position* in graphene Raman spectrum is located around 1560 cm^{-1}. A variation in the position of this peak may be attributed to electronic doping between the graphene and the substrate[42]. Finally *2D peak position* in graphene Raman spectrum (around 2700 cm^{-1}) should be displaced to lower Raman shift values if compared to that in graphite Raman spectrum (ranging from 2710 to 2720 cm^{-1}) [43].

It is important to note that 2D Raman band shape and position are good fingerprints that indicate the presence of monolayer, bilayer, few-layer and multilayer graphene samples. Thus, the 2D mode in bulk graphite, few-layer and multilayer graphene has been reported to be decomposed in two components [50]. Monolayer graphene has a single component. Nevertheless, the 2D Raman band in bilayer graphene is fitted to four components. Finally, although the Raman spectrum of graphene grown on metals shows fluorescence[50], this one has been treated using the SENTERRA Raman spectrometer software, thus allowing to clearly identify the different peaks appearing in the Raman spectrum.

Optical Microscopy

A SENTERRA X50 microscope equipped with the software OPUS was used to analyze the graphene samples. About 50 Optical Microscope images (132.4 µm*98.53 µm) were analyzed (although only six of them were considered as representative to be showed). In each image, four different colours were detected. It was checked that, dark orange colour would correspond with multilayer graphene, light orange colour was associated to few-layers graphene, yellow colour would correspond to bilayer graphene whereas white areas were associated to monolayer graphene.

Determination of the graphene *thickness value.* Thickness control.

A homemade Excel-VBA software application was designed with the aim of control the graphene thickness. This software was able to evaluate the percentage of the different types of graphene existing over a polycrystalline nickel foil by checking the different colours present in a digitalized Optical Microscope image. It was clearly demonstrated that, the different colours appearing in the Optical Microscope images were related to different types of graphene by using Raman spectroscopy (Figure 3). The Excel-VBA software application allowed to evaluate the percentage of each kind of graphene (multilayer, few-layer, bilayer and monolayer graphene) attending to its corresponding colour in the optical micrographs. For this purpose, a logarithmic scale (similar to that used for representing the pH in liquids) was considered. Thus, values 1, 10, 100 and 1000 were assigned to multilayer, few-layer, bilayer and monolayer graphene, respectively. The *thickness value* of the sheet was calculated as an average of the percentage obtained for each type of graphene[40].

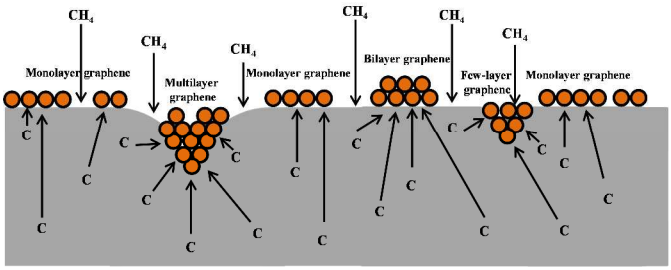

Fig 4: Mechanism graphene growth on polycrystalline nickel.

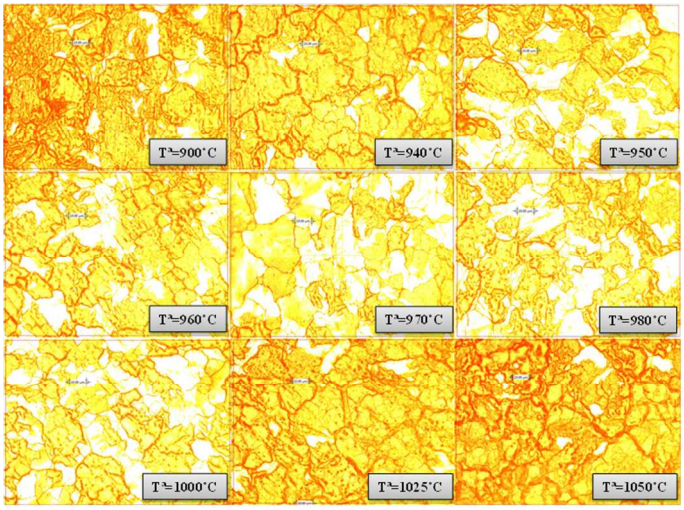

Fig 5. ***Influence of the reaction temperature***. Optical Microscopy images. (Synthesis conditions: 900-1050ºC, 600 s reaction time, CH_4/H_2 = 0.30 v/v, 130 Nml (CH_4+H_2)/min).

Results and discussion:

Influence of the reaction temperature:

In order to analyze the influence of the reaction temperature over the main characteristics of the synthesized graphene, different experiments were carried out by varying it between 900 and 1050 ºC. As it is well known, methane is a hydrocarbon with strong C-H bonds[51, 52]. Thus, the reaction temperature is considered a critical factor to be controlled during graphene synthesis then, high energy is needed to achieve methane dissociation. This dissociation is easier in Ni grain boundaries than in single crystal nickel surface since, in the former, higher chemical activation energy is required [53].

Figure 4 shows a diagram that represents the mechanism of graphene formation onto polycrystalline nickel, which involves two different steps. The first one is related to the absorption of C atoms into the bulk nickel or the incorporation of C atoms into the Ni substrate. The second one consists of the out-diffusion and/or adsorption of C atoms to the Ni surface[54]. As observed in Figure 4, the smooth parts of the polycrystalline Ni favors the growth of monolayer or bilayer graphene, while the rough surface with large amount of grain boundaries promotes the growth of multilayer graphene onto the nickel surface[39].

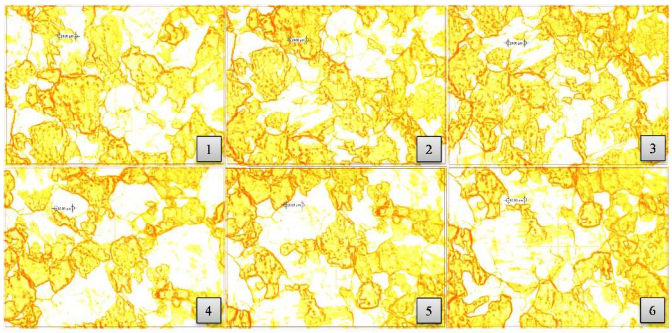

Fig 6. ***Influence of the reaction temperature.*** Optical Microscopy images corresponding to the sample synthesized at 980 ºC. (Synthesis conditions: 980ºC, 600 s reaction time, CH_4/H_2 = 0.3 v/v, 130 Nml (CH_4+H_2)/min).

Table 1. ***Influence of the reaction temperature***. Percentage of each type of graphene and *thickness values* corresponding to the sample synthesized at 980 ºC. (Synthesis conditions: 980 ºC, 600 s reaction time, CH_4/H_2 = 0.3 v/v, 130 Nml (CH_4+H_2)/min).

PICTURE	% MULTILAYER GRAPHENE	% FEW-LAYERS GRAPHENE	% BILAYER GRAPHENE	% MONOLAYER GRAPHENE	THICKNESS VALUE
1	0.57	36.56	20.05	42.82	451
2	1.10	44.33	24.44	30.12	330
3	0.68	49.57	26.88	22.86	260
4	0.75	32.43	17.04	49.78	518
5	1.06	37.10	19.33	42.51	448
6	1.02	41.23	23.06	34.69	374
AVERAGE	0.87	40.20	21.80	37.13	397

Figure 5 shows representative Optical Microscopy images of each sample obtained at different reaction temperatures. As observed, the orange color was more intense at both low (900-950 ºC) and high temperatures (1025-1050 ºC), indicating that multilayer graphene was mostly covering the sample. At intermediate temperatures, the color intensity decreased appearing lighter orange zones (few-layers graphene), yellow areas (bilayer graphene) and white areas (monolayer graphene), which was indicative of the deposition of thinner graphene.

In order to obtain a representative analysis of each synthesized sample, numerous pictures corresponding to different areas of the same graphene sample were analyzed by the EXCEL-VBA application previously described. As above mentioned, darker orange zones, including grain boundaries (characteristics of poly-crystalline Ni), were associated to multilayer graphene. Lighter orange areas were assigned to few-layers graphene. Yellow areas were associated to bilayer graphene. Finally, white areas were assigned to monolayer graphene. As an example of how to operate with all the synthesized samples, Figure 6 shows six representative Optical Microscope pictures and Table 1 the obtained results derived of them (percentages of each type of graphene) for sample synthesized at 980 ºC.

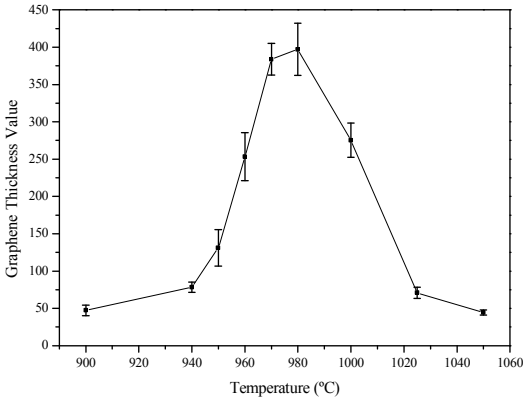

Fig 7. ***Influence of the reaction temperature***. Graphene *thickness value* vs temperature. Standard errors values have been also included. (Synthesis conditions: 900-1050ºC, 600 s reaction time, CH_4/H_2 = 0.3 v/v, 130 Nml (CH_4+H_2)/min).

Table 2. ***Influence of the reaction temperature***. Raman spectroscopy parameters and percentage of each type of graphene. (Synthesis conditions: 900-1050 ºC, 600 s reaction time, CH_4/H_2 = 0.3 v/v, 130 Nml (CH_4+H_2)/min).

INFLUENCE OF THE REACTION TEMPERATURE
(time = 600 s; CH_4/H_2=0.3 v/v; Q_T=130 Nml/min)

Tª (ºC)	TYPE OF GRAPHENE	%	I_D/I_G	I_{2D}/I_G	FWHM	2D RAMAN SHIFT (cm^{-1})	G RAMAN SHIFT (cm^{-1})
900	MONOLAYER	1.5	0.061	2.520	53	2703	1580
	BILAYER	25.8	0.013	0.976	69	2699	1580
	FEW-LAYER	62.9	0.013	0.599	74	2707	1580
	MULTILAYER	9.8	0.016	0.533	79	2703	1580
980	MONOLAYER	37.1	0.184	2.542	37	2705	1584
	BILAYER	21.8	0.006	1.007	42	2704	1584
	FEW-LAYER	40.2	0.001	0.346	74	2713	1584
	MULTILAYER	0.9	0.027	0.329	79	2708	1584
1050	MONOLAYER	1.5	0.007	2.230	58	3699	1580
	BILAYER	23.5	0.014	0.952	58	2707	1580
	FEW-LAYER	57.7	0.160	0.610	69	2703	1580
	MULTILAYER	17.3	0.015	0.410	74	2708	1580
OPTIMUM SAMPLE REPETITIVENESS							
980	MONOLAYER	37.5	0.180	2.623	38	2703	1584
	BILAYER	21.3	0.007	1.015	45	2705	1584
	FEW-LAYER	40.5	0.003	0.352	70	2713	1584
	MULTILAYER	0.7	0.025	0.315	76	2710	1584

Figure 7 summarizes the effect of the reaction temperature on the *thickness value* of the graphene deposited on Ni foils as well as the standard errors of each measurement. A maximum *thickness value* (397) was observed at 980 ºC, which was taken as a reference (optimum sample) in the following studies. As observed, Ni foil was covered with few-layer, bilayer and monolayer graphene obtaining a *thickness value* of 397 (Table 1).

Table 2 shows the main characteristic Raman parameters and the percentage of each type of graphene corresponding to graphene samples synthesized at three different reaction temperatures (900ºC, 980ºC (optimum Tª) and 1050ºC). These Raman parameters have been reported in the literature for each type of graphene[27, 36, 48, 55-59].

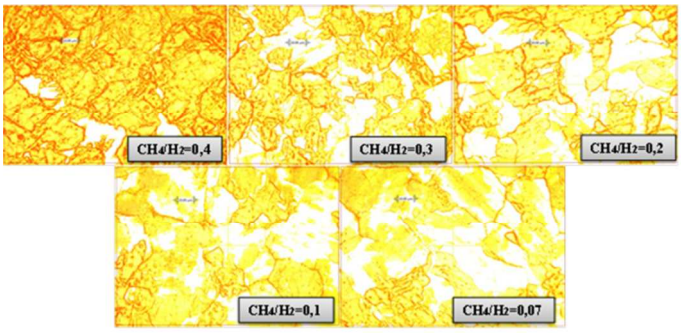

Fig 8. ***Influence of the CH_4/H_2 flow rate ratio.*** Optical Microscopy images. (Synthesis conditions: 980ºC, 600 s reaction time, CH_4/H_2 = 0.07-0.4 v/v, 130 Nml (CH_4+H_2)/min).

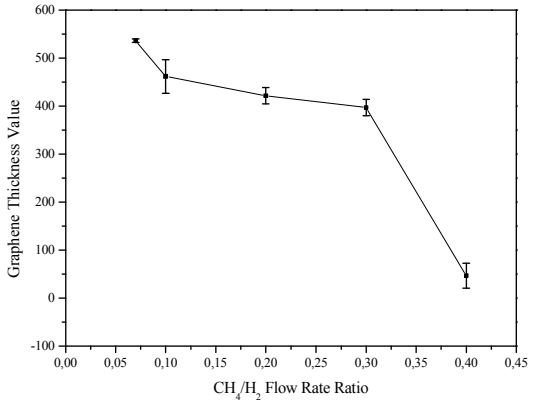

Fig 9. ***Influence of the CH_4/H_2 flow rate ratio.*** Graphene *thickness value* vs CH_4/H_2 flow rate ratio. Standard errors values have been also included. (Synthesis conditions: 980ºC, 600 s reaction time, CH_4/H_2 = 0.07-0.4 v/v, 130 Nml (CH_4+H_2)/min).

As observed, I_D/I_G ratio values were very low, indicating the absence of defects in the sample. On the other hand, I_{2D}/I_G ratio values were increased from the multilayer graphene to the monolayer one [60].

The contrary effect was observed when the parameter FWHM was analyzed. On the other hand, G and 2D peak positions were maintained constant in values around 1581 cm^{-1} and 2700 cm^{-1}, respectively [60, 42]. On the other hand, Table 2 also lists the characteristics Raman parameters of the optimum sample synthesized in a repetitiveness study. As observed, all Raman parameters remained practically constant, demonstrating that the synthesis process was reproducible. Furthermore, it can be observed that the best percentage of monolayer graphene was obtained at 980ºC, decreasing this percentage considerably at higher and lower temperatures. In the cases that the percentage of monolayer graphene was low, the one of few-layer and multilayer graphene increased, maintaining the percentage of bilayer graphene practically constant for all the temperatures.

Influence of the CH_4/H_2 flow rate ratio.

In order to analyze the influence of the CH_4/H_2 flow rate ratio over the main characteristics of the synthesized graphene, different experiments were carried out by varying it between 0.4 and 0.07 v/v.

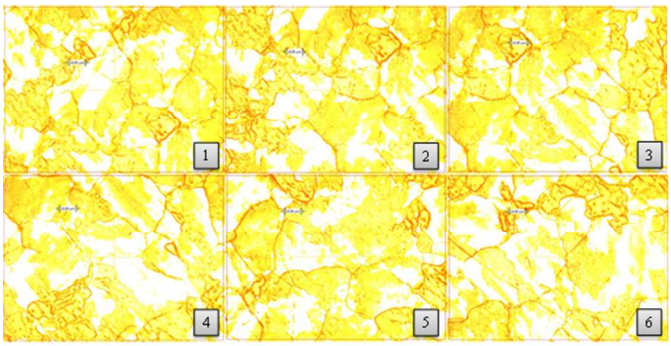

Fig 10. ***Influence of the CH_4/H_2 flow rate ratio.*** Optical Microscopy images corresponding to the sample synthesized using a CH_4/H_2 flow rate ratio value of 0.07 v/v. (Synthesis conditions: 980ºC, 600 s reaction time, CH_4/H_2 = 0.07 v/v, 130 Nml (CH_4+H_2)/min).

Table 3. ***Influence of the CH_4/H_2 flow rate ratio.*** Percentage of each type of graphene and *thickness values* corresponding to the sample synthesized using a CH_4/H_2 flow rate ratio value of 0.07 v/v. (Synthesis conditions: 980ºC, 600 s reaction time, CH_4/H_2 = 0.07 v/v, 130 Nml (CH_4+H_2)/min).

PICTURE	% MULTILAYER GRAPHENE	% FEW-LAYERS GRAPHENE	% BILAYER GRAPHENE	% MONOLAYER GRAPHENE	THICKNESS VALUE
1	0.25	23.65	21.50	54.60	569
2	0.52	29.32	22.10	48.05	505
3	0.45	33.46	25.09	41.00	438
4	0.17	21.37	17.80	60.66	606
5	0.83	32.07	20.56	46.54	489
6	0.52	23.03	15.32	61.13	608
AVERAGE	0.46	27.15	20.40	52.00	536

As mentioned, the amount of carbon precursor (CH_4) during the reaction, greatly determines the thickness of the synthesized graphene [52]. Ni acts as active catalyst dissolving a large quantity of carbon atoms. Thus, CH_4/H_2 flow rate ratio can successfully be used to control the carbon diffusion to the Ni surface, thus favoring monolayer or bilayer graphene formation[52, 61].

Figure 8 shows representative Optical Microscopy images of each sample obtained at different CH_4/H_2 flow rate ratios. As observed, orange color was more intense at higher CH_4/H_2 flow rate ratio values indicating that, samples were mainly covered by multilayer graphene. As the CH_4/H_2 flow rate ratios decrease, the color intensity decreased, appearing lighter orange zones (few-layer graphene), yellow areas (bilayer graphene) and white zones (monolayer graphene), highlighting the deposition of thinner graphene over the Ni foil.

Figure 9 summarizes the effect of the CH_4/H_2 flow rate ratio on the *thickness value* of the graphene deposited over Ni foils as well as the standard errors of each measurement. A maximum *thickness value* (536) was obtained for graphene synthesized using 0.07 v/v CH_4/H_2 flow rate ratio which was taken as a reference in the following studies.

Table 4. ***Influence of the CH_4/H_2 flow rate ratio.*** Raman spectroscopy parameters and percentage of each type of graphene. (Synthesis conditions: 980ºC, 600 s reaction time, CH_4/H_2 = 0.07-0.4 v/v, 130 Nml (CH_4+H_2)/min).

INFLUENCE OF THE CH_4/H_2 FLOW RATE RATIO (T^a=980ºC; time = 600 s; Q_T=130 Nml/min)							
CH_4/H_2 (v/v)	TYPE OF GRAPHENE	%	I_D/I_G	I_{2D}/I_G	FWHM	2D RAMAN SHIFT (cm^{-1})	G RAMAN SHIFT (cm^{-1})
0.4	MONOLAYER	1.5	0.058	1.960	53	2707	1584
	BILAYER	25.1	0.045	0.941	58	2695	1584
	FEW-LAYER	61.3	0.004	0.415	74	2713	1584
	MULTILAYER	12.1	0.004	0.405	79	2708	1584
0.2	MONOLAYER	34.7	0.034	2.021	42	2695	1581
	BILAYER	20.8	0.043	1.296	47	2707	1581
	FEW-LAYER	38.3	0.010	0.473	63	2713	1581
	MULTILAYER	6.2	0.001	0.415	63	2713	1581
0.07	MONOLAYER	51.9	0.142	2.159	40	2707	1581
	BILAYER	20.4	0.027	1.136	53	2700	1581
	FEW-LAYER	27.1	0.006	0.435	69	2709	1581
	MULTILAYER	0.6	0.062	0.429	74	2704	1581
OPTIMUM SAMPLE REPETITIVENESS							
0.07	MONOLAYER	50.2	0.145	2.045	46	2707	1581
	BILAYER	22.5	0.021	1.162	55	2700	1581
	FEW-LAYER	26.7	0.005	0.420	70	2705	1581
	MULTILAYER	0.6	0.059	0.462	72	2700	1581

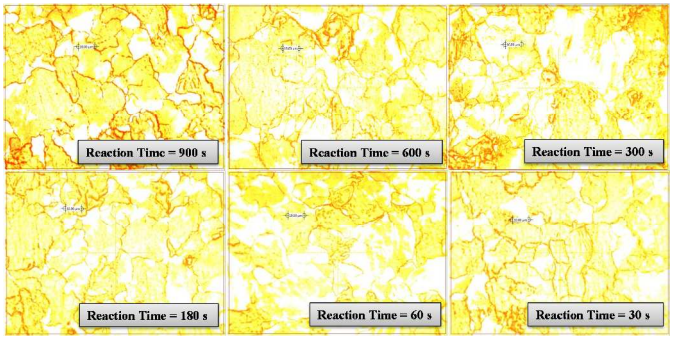

Fig 11. ***Influence reaction time.*** Optical Microscopy images. (Synthesis conditions: 980ºC, 900-30 s reaction time, CH_4/H_2 = 0.07 v/v, 130 Nml (CH_4+H_2)/min).

Figure 10 shows six representative Optical Microscopy pictures and Table 3 the obtained results derived of them (percentages of each type of graphene) for sample synthesized using a CH_4/H_2 flow rate ratio value of 0.07 v/v. As observed, as the CH_4/H_2 flow rate ratio decrease, the percentage of few-layer graphene decreased and, the one corresponding to monolayer graphene increased. By its part, the percentage of bilayer graphene was kept practically constant. Consequently, the *thickness value* increased from 397 (sample synthesized by using a CH_4/H_2 flow rate ratio value of 0.3 v/v) to 536 (sample synthesized by using a CH_4/H_2 flow rate ratio value of 0.07 v/v).

Table 4 shows the main characteristic Raman parameters and the percentage of each type of graphene corresponding to graphene samples synthesized at three different values of the CH_4/H_2 flow rate ratios (0.4 v/v, 0.2 v/v and 0.07 v/v).

As observed, I_D/I_G ratio values were, in all cases, very low indicating the absence of defects in the sample. On the other hand, I_{2D}/I_G ratio

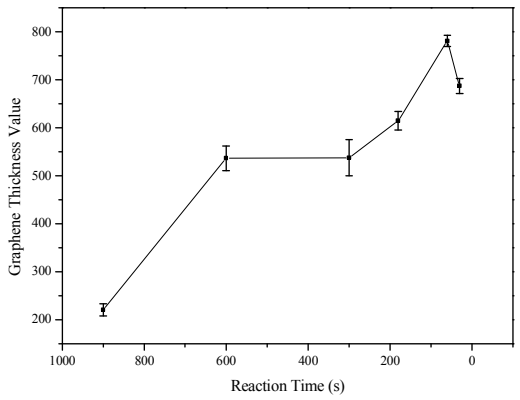

Fig 12. ***Influence reaction time.*** Graphene *thickness value* vs reaction time. Standard errors values have been also included. (Synthesis conditions: 980ºC, 900-30 s reaction time, CH_4/H_2 = 0.07 v/v, 130 Nml (CH_4+H_2)/min).

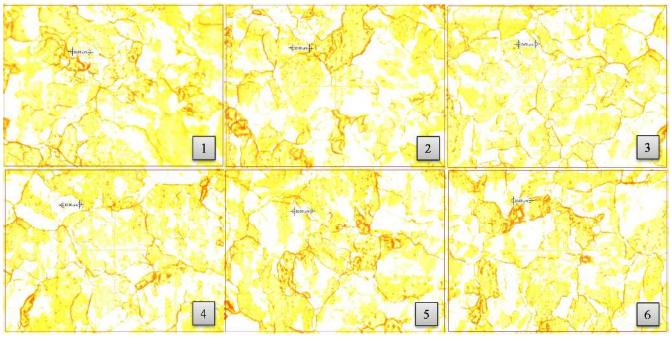

Fig 13. ***Influence reaction time.*** Optical Microscopy images corresponding to the sample synthesized during 60 seconds of reaction time. (Synthesis conditions: 980ºC, 60 s reaction time, CH_4/H_2 = 0.07 v/v, 130 Nml (CH_4+H_2)/min).

values increased and FWHM values decreased from the multilayer graphene to the monolayer one [60]. Finally, G and 2D peaks were located around 1581 cm^{-1} and 2700 cm^{-1}, respectively [60, 42]. Note that, Table 4 also lists the characteristics Raman parameters of the optimum sample synthesized in a repetitiveness study. As observed, all Raman parameters remained practically constant, demonstrating that the synthesis process was reproducible. Additionally, it can be observed that the highest percentage of monolayer graphene was obtained by using a CH_4/H_2 flow rate ratio of 0.07 v/v.

Influence of the reaction time

In order to analyze the influence of the reaction time over the main characteristics of the synthesized graphene, different experiments were carried out varying it between 30 and 900 seconds, keeping constant the rest of operational parameters (980ºC, 900-30 s reaction time, CH_4/H_2 = 0.07 v/v, 130 Nml (CH_4+H_2)/min).

Figure 11 shows the Optical Microscopy images of each sample obtained at different reaction times. As observed, orange color was present in a higher extend at higher reaction times (> 5 min), indicating that those samples were mainly covered by multilayer and/or few layer graphene which has been attributed to the longer exposition of the Ni foil to the carbonaceous precursor. In general, at lower reaction times the presence of white zones (related to monolayer graphene), were increased highlighting the deposition of thinner graphene over the Ni foil.

Table 5. ***Influence of the reaction time.*** Percentage of each type of graphene and *thickness values* corresponding to the sample synthesized during 60 seconds of reaction time. (Synthesis conditions: 980ºC, 60 s reaction time, CH_4/H_2 = 0.07 v/v, 130 Nml (CH_4+H_2)/min).

PICTURE	% MULTILAYER GRAPHENE	% FEW-LAYERS GRAPHENE	% BILAYER GRAPHENE	% MONOLAYER GRAPHENE	THICKNESS VALUE
1	0.03	12.11	13.06	74.80	762.20
2	0.08	11.26	11.70	76.96	782.50
3	0.02	7.35	9.40	83.24	842.50
4	0.21	12.38	10.91	76.50	777.10
5	0.28	13.40	11.32	75.00	762.70
6	0.10	13.42	11.84	74.65	759.70
AVERAGE	0.12	11.65	11.37	76.86	781

Table 6. ***Influence reaction time***. Raman spectroscopy parameters and percentage of each type of graphene. (Synthesis conditions: 980ºC, 900-30 s reaction time, CH_4/H_2 = 0.07 v/v, 130 Nml (CH_4+H_2)/min).

INFLUENCE OF THE REACTION TIME (T^a=980ºC; CH_4/H_2=0.07 (v/v); Q_T=130 Nml/min)							
Time (s)	TYPE OF GRAPHENE	%	I_D/I_G	I_{2D}/I_G	FWHM	2D RAMAN SHIFT (cm^{-1})	G RAMAN SHIFT (cm^{-1})
900	MONOLAYER	18.2	0.086	2.185	42	2702	1581
	BILAYER	33.7	0.010	0.969	47	2707	1581
	FEW-LAYER	47.2	0.025	0.356	79	2710	1581
	MULTILAYER	0.9	0.035	0.335	84	2709	1581
60	MONOLAYER	76.8	0.015	2.513	32	2703	1581
	BILAYER	11.3	0.016	1.413	47	2699	1581
	FEW-LAYER	11.6	0.006	0.569	63	2707	1581
	MULTILAYER	0.3	0.007	0.49	74	2708	1584
30	MONOLAYER	67.1	0.067	1.917	47	2703	1581
	BILAYER	14.7	0.077	1.187	58	2707	1581
	FEW-LAYER	18.1	0.055	0.557	68	2709	1581
	MULTILAYER	0.1	0.019	0.505	79	2708	1581
OPTIMUM SAMPLE REPETITIVENESS							
60	MONOLAYER	79.5	0.014	2.503	35	2703	1581
	BILAYER	10.2	0.015	1.402	45	2700	1581
	FEW-LAYER	9.9	0.010	0.612	60	2700	1581
	MULTILAYER	0.4	0.008	0.465	70	2703	1581

Figure 12 summarizes the effect of the reaction time over the *thickness value* of the graphene deposited over Ni foils. A maximum *thickness value* (781) was observed at 60 seconds of reaction time. This reaction time was considered as the optimum to obtain the best quality graphene. Figure 13 shows six representative Optical Microscopy pictures and Table 5, the obtained results derived of them (percentages of each type of graphene) for sample synthesized during 60 seconds of reaction time. As it could be clearly observed, the *thickness value* increased up from 536 (sample synthesized by using a reaction time of 600 s) to 781 (sample synthesized by using a reaction time of 60 s). Note that, the percentage of monolayer graphene reached a value of 77%, the highest one obtained in the present study.

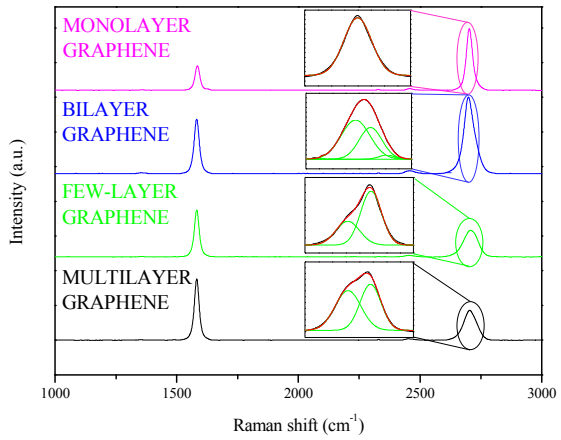

Fig 14: ***Influence reaction time.*** Raman spectrum and 2D peak deconvolution corresponding to the sample synthesized during 60 seconds of reaction time. (Synthesis conditions: 980ºC, 60 s reaction time, CH_4/H_2 = 0.07 v/v, 130 Nml (CH_4+H_2)/min).

Table 6 shows the main characteristic Raman parameters and those of the repetition (T[a]=980ºC, 60 s reaction time, CH_4/H_2 = 0.07, 130 Nml (CH_4+H_2)/min) corresponding to graphene samples synthesized at three different reaction times including also, the percentage of each type of graphene. Again, I_D/I_G ratio values were very low and, I_{2D}/I_G ratio values increased from the multilayer graphene to the monolayer one[60] (note that I_{2D}/I_G ratio value corresponding to the sample synthesized during 60 s of reaction time was the highest one). FWHM values decreased from the multilayer graphene to the monolayer one[60]. On the other hand, G and 2D peaks were located around 1581 cm^{-1} and 2700 cm^{-1}, respectively [60, 42]. Respect to the repetitiveness of the synthesis procedure, again all characteristics Raman parameters remained almost inalterable, demonstrating that the synthesis process was reproducible. Note that, the highest percentage of monolayer graphene was obtained when the graphene synthesis was carried out during 60 s of reaction time.

Figure 14 plots the four Raman Spectrum characteristic of the optimum sample (synthesis conditions: 980ºC, 60 s reaction time, CH_4/H_2 = 0.07, 130 Nml (CH_4+H_2)/min), and the corresponding 2D peak deconvolution for each type of graphene. As expected, 2D peak, corresponding to monolayer graphene was fitted with a symmetric and sharp single peak; 2D peak, corresponding to bilayer graphene, was deconvoluted in four contributions. Finally, 2D peak deconvolution corresponding with few-layers and multilayer graphene presented two different contributions similar as those observed for graphite.

Conclusions

The aim of this work was to optimize the graphene growth over polycrystalline nickel foils using a homemade atmospheric pressure Chemical Vapor Deposition setup. A cheaper alternative to synthesize high quality graphene is considered by using polycrystalline Ni foils instead of single crystal. CH_4 was used as the precursor gas whereas H_2 and N_2 were used as carrier gases. Three different growth parameters affecting the CVD-grown graphene characteristics, e.g. reaction temperature, CH_4/H_2 flow rate ratio and reaction time, were studied in detail.

It was observed that synthesized graphene do not homogeneously grow over the entire Ni foil and four different types of graphene (e.g. monolayer, bilayer, few-layer and multilayer) were deposited, as indicated the different colors in the Optical Microscope images. It was observed a maximum of the *thickness value* (781) for a temperature, a CH_4/H_2 flow rate ratio and a reaction time of 980 ºC, 0.07 v/v and 60 seconds, respectively. At these conditions, about 77% of the Ni foil was covered with monolayer graphene.

Acknowledgements

The authors acknowledge financial support from the Spanish company Graphenano Nanotechnologies.

Notes and references

[a] Department of Chemical Engineering, University of Castilla-La Mancha, Avda. Camilo José Cela 12, Ciudad Real, Spain, 13071..
[b] Department of Chemical Engineering, University of Castilla-La Mancha, Avda. Camilo José Cela 12, Ciudad Real, Spain, 13071.

1. K. S. Novoselov, A. K. Geim, S. V. Morozov, D. Jiang, Y. Zhang, S. V. Dubonos, I. V. Grigorieva and A. A. Firsov, *Science*, 2004, **306**, 666-669.
2. K. S. Novoselov, A. K. Geim, S. V. Morozov, D. Jiang, M. I. Katsnelson, I. V. Grigorieva, S. V. Dubonos and A. A. Firsov, *Nature*, 2005, **438**, 197-200.
3. A. K. Geim and K. S. Novoselov, *Nat. Mater.*, 2007, **6**, 183-191.
4. A. K. Geim, *Science*, 2009, **324**, 1530-1534.
5. Y. Y. Wang, Z. H. Ni, T. Yu, Z. X. Shen, H. M. Wang, Y. H. Wu, W. Chen and A. T. S. Wee, *J. Phys. Chem. C*, 2008, **112**, 10637-10640.
6. H. K. Chae, D. Y. Siberio-Pérez, J. Kim, Y. Go, M. Eddaoudi, A. J. Matzger, M. O'Keeffe and O. M. Yaghi, *Nature*, 2004, **427**, 523-527.
7. L. X. Dong and Q. Chen, *Signal Image Video Process.*, 2010, **4**, 45-51.
8. L. S. Schadler, S. C. Giannaris and P. M. Ajayan, *Appl. Phys. Lett.*, 1998, **73**, 3842-3844.
9. Y. Zhu, S. Murali, W. Cai, X. Li, J. W. Suk, J. R. Potts and R. S. Ruoff, *Adv. Mater.*, 2010, **22**, 3906-3924.
10. N. Li, Z. Wang, K. Zhao, Z. Shi, Z. Gu and S. Xu, *Carbon*, 2010, **48**, 1580-1585.
11. S. Karmakar, N. V. Kulkarni, A. B. Nawale, N. P. Lalla, R. Mishra, V. G. Sathe, S. V. Bhoraskar and A. K. Das, *J. Phys. D: Appl. Phys.*, 2009, **42**.
12. E. Rollings, G. H. Gweon, S. Y. Zhou, B. S. Mun, J. L. McChesney, B. S. Hussain, A. V. Fedorov, P. N. First, W. A. de Heer and A. Lanzara, *J. Phys. Chem. Solids*, 2006, **67**, 2172-2177.
13. W. A. de Heer, C. Berger, X. Wu, P. N. First, E. H. Conrad, X. Li, T. Li, M. Sprinkle, J. Hass, M. L. Sadowski, M. Potemski and G. Martinez, *Solid State Commun.*, 2007, **143**, 92-100.
14. Z. H. Ni, W. Chen, X. F. Fan, J. L. Kuo, T. Yu, A. T. S. Wee and Z. X. Shen, *Phys. Rev. B Condens. Matter Mater. Phys.*, 2008, **77**.
15. P. W. Sutter, J. I. Flege and E. A. Sutter, *Nat. Mater.*, 2008, **7**, 406-411.
16. T. Seyller, A. Bostwick, K. V. Emtsev, K. Horn, L. Ley, J. L. McChesney, T. Ohta, J. D. Riley, E. Rotenberg and F. Speck,

Physica Status Solidi (B) Basic Research, 2008, **245**, 1436-1446.
17. M. Sprinkle, P. Soukiassian, W. A. De Heer, C. Berger and E. H. Conrad, *Physica Status Solidi Rapid Res. Lett.*, 2009, **3**, A91-A94.
18. D. V. Kosynkin, A. L. Higginbotham, A. Sinitskii, J. R. Lomeda, A. Dimiev, B. K. Price and J. M. Tour, *Nature*, 2009, **458**, 872-876.
19. A. Hirsch, *Angewandte Chemie - International Edition*, 2009, **48**, 6594-6596.
20. L. Jiao, L. Zhang, X. Wang, G. Diankov and H. Dai, *Nature*, 2009, **458**, 877-880.
21. C. D. Kim, B. K. Min and W. S. Jung, *Carbon*, 2009, **47**, 1610-1612.
22. X. Yang, X. Dou, A. Rouhanipour, L. Zhi, H. J. Räder and K. Müllen, *J. Am. Chem. Soc.*, 2008, **130**, 4216-4217.
23. W. Zhang, J. Cui, C. A. Tao, Y. Wu, Z. Li, L. Ma, Y. Wen and G. Li, *Angewandte Chemie - International Edition*, 2009, **48**, 5864-5868.
24. X. Wang, H. You, F. Liu, M. Li, L. Wan, S. Li, Q. Li, Y. Xu, R. Tian, Z. Yu, D. Xiang and J. Cheng, *Chem. Vap. Deposition*, 2009, **15**, 53-56.
25. Y. Wang, X. Chen, Y. Zhong, F. Zhu and K. P. Loh, *Appl. Phys. Lett.*, 2009, **95**.
26. E. Dervishi, Z. Li, F. Watanabe, A. Biswas, Y. Xu, A. R. Biris, V. Saini and A. S. Biris, *Chem. Commun.*, 2009, 4061-4063.
27. X. Li, W. Cai, J. An, S. Kim, J. Nah, D. Yang, R. Piner, A. Velamakanni, I. Jung, E. Tutuc, S. K. Banerjee, L. Colombo and R. S. Ruoff, *Science*, 2009, **324**, 1312-1314.
28. S. J. Chae, F. Güneş, K. K. Kim, E. S. Kim, G. H. Han, S. M. Kim, H. Shin, S. M. Yoon, J. Y. Choi, M. H. Park, C. W. Yang, D. Pribat and Y. H. Lee, *Advanced Materials*, 2009, **21**, 2328-2333.
29. K. A. Worsley, P. Ramesh, S. K. Mandal, S. Niyogi, M. E. Itkis and R. C. Haddon, *Chem. Phys. Lett.*, 2007, **445**, 51-56.
30. A. N. Obraztsov, *Nat Nanotechnol*, 2009, **4**, 212-213.
31. K. V. Emtsev, A. Bostwick, K. Horn, J. Jobst, G. L. Kellogg, L. Ley, J. L. McChesney, T. Ohta, S. A. Reshanov, J. Röhrl, E. Rotenberg, A. K. Schmid, D. Waldmann, H. B. Weber and T. Seyller, *Nat. Mater.*, 2009, **8**, 203-207.
32. S. Bae, H. Kim, Y. Lee, X. Xu, J. S. Park, Y. Zheng, J. Balakrishnan, T. Lei, H. Ri Kim, Y. I. Song, Y. J. Kim, K. S. Kim, B. Özyilmaz, J. H. Ahn, B. H. Hong and S. Iijima, *Nat Nanotechnol*, 2010, **5**, 574-578.
33. K. S. Kim, Y. Zhao, H. Jang, S. Y. Lee, J. M. Kim, J. H. Ahn, P. Kim, J. Y. Choi and B. H. Hong, *Nature*, 2009, **457**, 706-710.
34. G. A. López and E. J. Mittemeijer, *Scripta Mater.*, 2004, **51**, 1-5.
35. A. Umair and H. Raza, *Nanoscale Res. Lett.*, 2012, **7**.
36. G. Ruan, Z. Sun, Z. Peng and J. M. Tour, *ACS Nano*, 2011, **5**, 7601-7607.
37. Z. Sun, Z. Yan, J. Yao, E. Beitler, Y. Zhu and J. M. Tour, *Nature*, 2010, **468**, 549-552.
38. M. H. Rümmeli, C. G. Rocha, F. Ortmann, I. Ibrahim, H. Sevincli, F. Börrnert, J. Kunstmann, A. Bachmatiuk, M. Pötschke, M. Shiraishi, M. Meyyappan, B. Büchner, S. Roche and G. Cuniberti, *Adv. Mater.*, 2011, **23**, 4471-4490.
39. Y. Zhang, L. Gomez, F. N. Ishikawa, A. Madaria, K. Ryu, C. Wang, A. Badmaev and C. Zhou, *J. Phys. Chem. Lett.*, 2010, **1**, 3101-3107.
40. M. P. Lavin-Lopez, J. L. Valverde, M. C. Cuevas, A. Garrido, L. Sanchez-Silva, P. Martinez and A. Romero-Izquierdo, *PCCP*, 2014, **16**, 2962-2970.
41. A. Dahal and M. Batzill, *Nanoscale*, 2014, **6**, 2548-2562.
42. A. C. Ferrari, J. C. Meyer, V. Scardaci, C. Casiraghi, M. Lazzeri, F. Mauri, S. Piscanec, D. Jiang, K. S. Novoselov, S. Roth and A. K. Geim, *Phys. Rev. Lett.*, 2006, **97**.
43. I. Calizo, D. Teweldebrhan, W. Bao, F. Miao, C. N. Lau and A. A. Balandin, *Journal of Physics: Conference Series*, 2008, **109**, 5.
44. A. Das, B. Chakraborty and A. K. Sood, *Bull. Mater. Sci.*, 2008, **31**, 579-584.
45. C. N. R. Rao, U. Maitra and H. S. S. R. Matte, Wiley-VCH, 2012, pp. 1-47.
46. M. Wall, *Adv. Mater. Processes*, 2012, **170**, 35-38.
47. J. W. Suk, A. Kitt, C. W. Magnuson, Y. Hao, S. Ahmed, J. An, A. K. Swan, B. B. Goldberg and R. S. Ruoff, *ACS Nano*, 2011, **5**, 6916-6924.
48. A. Reina, X. Jia, J. Ho, D. Nezich, H. Son, V. Bulovic, M. S. Dresselhaus and K. Jing, *Nano Lett.*, 2009, **9**, 30-35.
49. Y. Gong, X. Zhang, G. Liu, L. Wu, X. Geng, M. Long, X. Cao, Y. Guo, W. Li, J. Xu, M. Sun, L. Lu and L. Liu, *Adv. Funct. Mater.*, 2012, **22**, 3153-3159.
50. S. D. Costa, A. Righi, C. Fantini, Y. Hao, C. Magnuson, L. Colombo, R. S. Ruoff and M. A. Pimenta, *Solid State Commun.*, 2012, **152**, 1317-1320.
51. Z. Chen, W. Ren, B. Liu, L. Gao, S. Pei, Z. S. Wu, J. Zhao and H. M. Cheng, *Carbon*, 2010, **48**, 3543-3550.
52. C. Z. C. Miao, O. Liang and Y. H. Xie *Chemical Vapor Deposition of Graphene, Physics and Applications of Graphene - Experiments*, 2011.
53. C. Z. C. Miao, O. Liang and Y. H. Xie, 2011.
54. M. Losurdo, M. M. Giangregorio, P. Capezzuto and G. Bruno, *PCCP*, 2011, **13**, 20836-20843.
55. J. Y. Hwang, C. C. Kuo, L. C. Chen and K. H. Chen, *Nanotechnology*, 2010, **21**.
56. C. Mattevi, H. Kim and M. Chhowalla, *J. Mater. Chem.*, 2011, **21**, 3324-3334.
57. S. Chen, W. Cai, R. D. Piner, J. W. Suk, Y. Wu, Y. Ren, J. Kang and R. S. Ruoff, *Nano Lett.*, 2011, **11**, 3519-3525.
58. S. Lee, K. Lee and Z. Zhong, *Nano Lett.*, 2010, **10**, 4702-4707.
59. D. Lee, K. Lee, S. Jeong, J. Lee, B. Choi and O. Kim, *Japanese Journal of Applied Physics*, 2012, **51**.
60. R. J. Nemanich and S. A. Solin, *Physical Review B*, 1979, **20**, 392-401.
61. R. S. Weatherup, B. Dlubak and S. Hofmann, *ACS Nano*, 2012, **6**, 9996-10003.